Nitrogen-Doped Anatase Nanofibers Decorated with Noble Metal Nanoparticles for Photocatalytic Production of Hydrogen

Ming-Chung Wu,[†,¶] Jussi Hiltunen,[‡] András Sápi,[§] Anna Avila,[‡] William Larsson,[▽] Hsueh-Chung Liao,[¶] Mika Huuhtanen,[‡] Géza Tóth,[†] Andrey Shchukarev,[▽] Noémi Laufer,[§] Ákos Kukovecz,[§] Zoltán Kónya,[§] Jyri-Pekka Mikkola,[▽,∥] Riitta Keiski,[‡] Wei-Fang Su,[¶] Yang-Fang Chen,[#] Heli Jantunen,[†] Pulickel M. Ajayan,[▲] Robert Vajtai,[▲,*] and Krisztián Kordás[†,▽]

[†]Microelectronics and Materials Physics Laboratories, Department of Electrical and Information Engineering and [‡]Mass and Heat Transfer Process Laboratory, Department of Process and Environmental Engineering, University of Oulu, P.O. Box 4500, Oulu FIN-90014, Finland, [§]Department of Applied and Environmental Chemistry, University of Szeged, 6720 Szeged, Rerrich Béla tér 1, Hungary, [∥]Industrial Chemistry and Reaction Engineering, Process Chemistry, Centre, Åbo Akademi University, Biskopsgata 8 FI-20500 Åbo-Turku, Finland, [¶]Department of Materials Science and Engineering, National Taiwan University, Taipei 106-17, Taiwan, [#]Department of Physics, National Taiwan University, Taipei, Taiwan, [▲]Department of Materials Science and Engineering, Rice University, Houston, Texas 77005, United States, and [▽]Technical Chemistry, Department of Chemistry, Chemical-Biological Center, Umeå University, SE-901 87 Umeå, Sweden

The discovery of photoelectrochemical splitting of water on titanium dioxide (TiO_2) by Fujishima and Honda in 1972 has initiated a considerable boom of semiconductor-based photocatalyst research.[1] Despite the nearly 40 years history of the topic, TiO_2 and its derivatives are still in the mainstream of the studies because of their availability, low cost, good and tunable photocatalytic activity, and photostability enabling versatile applications in a number of different fields such as air purification,[2,3] wastewater treatment,[4,5] hydrogen generation,[6−8] and antimicrobial coatings,[9,10] among many others. A great deal of photocatalyst research has been carried out to customize the electronic band structure of the semiconducting materials for a specific chemical process.[11,12] In the case of water cleavage, the goal has always been to find materials with band structure, allowing high energy transitions needed for the electrons/holes in reductive/oxidative processes, yet having it low enough to enable electron−hole pair generation with optical photons preferable in the visible spectrum. In the case of pristine TiO_2, one drawback is the too large band gap of $E_g \sim$ 3.2 eV, which restricts applications mainly with UV photons.[12]

Asahi et al.[13] reported that nitrogen doping can decrease the band gap of n-type TiO_2 due to the mixing of N 2p states with O

ABSTRACT We report the synthesis of N-doped TiO_2 nanofibers and high photocatalytic efficiency in generating hydrogen from ethanol−water mixtures under UV-A and UV-B irradiation. Titanate nanofibers synthesized by hydrothermal method are annealed in air and/or ammonia to achieve N-doped anatase fibers. Depending on the synthesis route, either interstitial N atoms or new N—Ti bonds appear in the lattice, resulting in slight lattice expansion as shown by XPS and HR-TEM analysis, respectively. These nanofibers were then used as support for Pd and Pt nanoparticles deposited with wet impregnation followed by calcination and reduction. In the hydrogen generation tests, the N-doped samples were clearly outperforming their undoped counterparts, showing remarkable efficiency not only under UV-B but also with UV-A illumination. When 100 mg of catalyst (N-doped TiO_2 nanofiber decorated with Pt nanoparticles) was applied to 1 L of water−ethanol mixture, the H_2 evolution rates were as high as 700 μmol/h (UV-A) and 2250 μmol/h (UV-B) corresponding to photo energy conversion percentages of ∼3.6 and ∼12.3%, respectively.

KEYWORDS: hydrogen production · photocatalysis · nanowire · nitrogen-doped anatase

2p states and shown photodegradation of methylene blue and gaseous acetaldehyde with photons of the visible spectrum. As it has been demonstrated later, substitution of O in the lattice with C leads to a similar result.[11,12,14] A further improvement of photocatalytic performance can be obtained by decorating the n-type semiconducting TiO_2 and its derivatives with metals of large work function[3,9,10,15−17] or with other semiconducting materials[18−20] having different band structure (p-type doping, nearly intrinsic behavior or much smaller band gap). In the former case, a Schottky
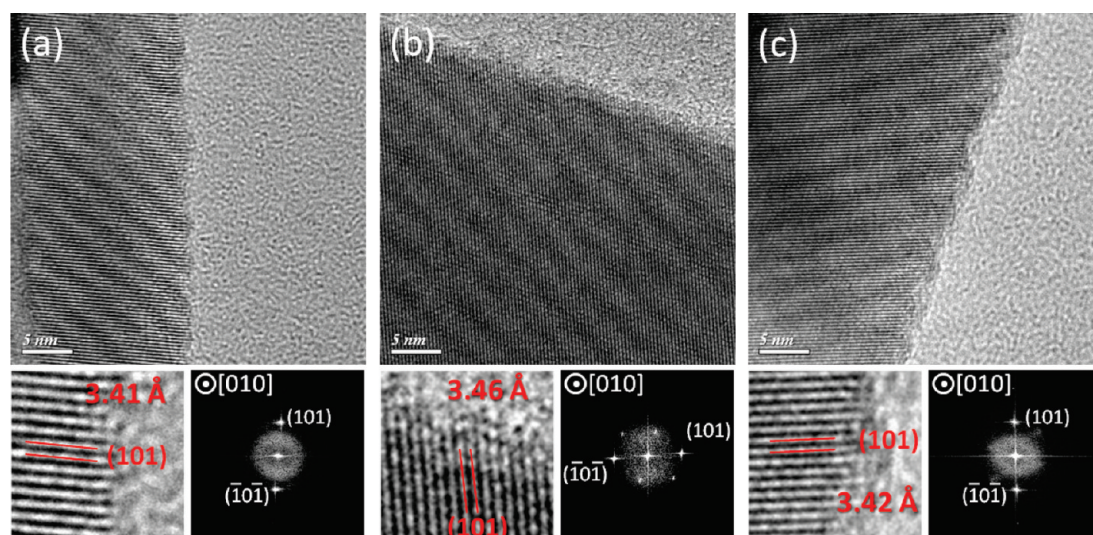
Figure 1. TEM images of (a) pristine TiO_2 NF, (b) N-TiO_2(A) NF, and (c) N-TiO_2(B) NF. Panels in the bottom right corners show high-magnification images of the lattice with the corresponding fast Fourier transformed pattern of each sample.

interface forms between the metal nanoparticle and the n-type TiO_2, while in the latter one, a p−n junction might evolve at the interface. As both types of junctions have rectifying electrical transport behavior, efficient charge separation of the photogenerated electron−hole pairs is achieved, which disables the undesired electron−hole recombination.[21−25]

In the present study, we are combining the efforts of lattice doping and metal nanoparticle decoration with the recent achievements of titanate/titania nanofiber synthesis[26,27] in order to develop novel and efficient photocatalyst materials that are easy to produce even in industrial quantities. The reason for applying nanofiber-based catalysts is the versatility of postprocessing such materials because with the elongated nanoparticles it is relatively simple to form large area films, coatings, and porous membranes as well as composites with polymers,[25,27] all which would be practical in the chemical processes listed above.[2−10] Accordingly, here we report on the synthesis of nitrogen-doped TiO_2 nanofibers (N-TiO_2 NFs) and their metal (Pt and Pd)-decorated derivatives and demonstrate for the first time an ultraefficient H_2 generation from water−ethanol mixtures under UV-A and UV-B irradiation. To our best knowledge, this is the first study to use N-TiO_2 NFs and its metal-decorated derivatives for hydrogen generation.

RESULTS AND DISCUSSION

We report here two kinds of nitrogen-doped TiO_2 nanofibers, referred as N-TiO_2(A) NF and N-TiO_2(B) NF, synthesized using different calcination methods: N-TiO_2(A) NF is synthesized by the calcination of $H_{2−x}Na_xTi_yO_{2y+1}$ nanofibers at 600 °C in ammonia gas flow (50 mL/min, 2% NH_3 in N_2 buffer) for 15 h, while N-TiO_2(B) NF is synthesized also from $H_{2−x}Na_xTi_yO_{2y+1}$ but in two subsequent calcination

steps: first, calcined in air at 600 °C for 12 h to form TiO_2 anatase nanofibers, followed by a second calcination step in ammonia gas (50 mL/min, 2% NH_3 in N_2 buffer) at the same temperature for 3 h.

After the annealing processes, both products have different colors than the undoped material. While the undoped material is a white powder, N-TiO_2(A) NFs are bluish and N-TiO_2(B) NFs appear as a pale gray color (see the Supporting Information, Figure S1). High-resolution TEM images of pristine TiO_2 NF and nitrogen-doped TiO_2 nanofibers (Figure 1) show that the calcination processes were sufficient to form a highly crystalline anatase structure with both routes. An increased d spacing for the (101) crystal plane is observed only for the N-TiO_2(A) samples, suggesting that the one-step calcination method resulted in incorporation of interstitial N atoms into the lattice,[28] while the two-step calcination method introduced the nitrogen atoms onto substitutional locations. In N-TiO_2(A) NFs (titanate annealed in NH_3 at 600 °C for 15 h), the change of (101) spacing is from 3.41 to 3.46 Å; however, in N-TiO_2(B) NFs, no considerable expansion of the lattice is visible (Figure 1).

The two different high-temperature treatments in NH_3 result in nitrogen doping of the raw materials as calculated from N 1s XPS spectra (Table 1). The N 1s component at 397.8 eV of N-TiO_2 (A) NF can be assigned to interstitial nitrogen atoms (N/Ti ratio of 0.0111), while the peak at 396.3 eV of N-TiO_2 (B) NF is due to substitutional nitrogen (formed Ti−N bond, N/Ti ratio of 0.0021).[29] The other components with higher binding energies (>399.0 eV) detected for each sample correspond to decomposition products of NH_3 molecules and/or other surface contamination. The difference in the N/Ti atomic ratios measured for the interstitial and substitutional nitrogen is reasonable considering the different synthesis condition. It is

TABLE 1. XPS Peak Positions, Element Concentration, and N/Ti Ratio in TiO₂ NF, N-TiO₂(A) NF, and N-TiO₂(B) NF Samples

sample	N 1s peak position and concentration (the corresponding N/Ti ratio)			Ti 2p$_{3/2}$ peak position and concentration	O 1s peak position and concentration		
TiO₂ NF	not detected	399.0 eV; 0.08 at % (0.0031)	400.4 eV; 0.30 at % (0.0118)	458.5 eV; 25.47 at %	529.7 eV; 50.87 at %	530.7 eV; 4.02 at %	531.7 eV; 3.28 at %
N-TiO₂(A) NF	397.8 eV; 0.28 at % (0.0111)	400.6 eV; 0.19 at % (0.0076)	401.9 eV; 0.08 at % (0.0031)	458.5 eV; 25.24 at %	529.7 eV; 48.62 at %	530.6 eV; 6.05 at %	531.8 eV; 1.85 at %
N-TiO₂(B) NF	396.3 eV; 0.05 at % (0.0021)	399.3 eV; 0.18 at % (0.0072)	401.2 eV; 0.11 at % (0.0044)	458.5 eV; 25.08 at %	529.8 eV; 50.18 at %	531.1 eV; 4.41 at %	532.1 eV; 1.41 at %
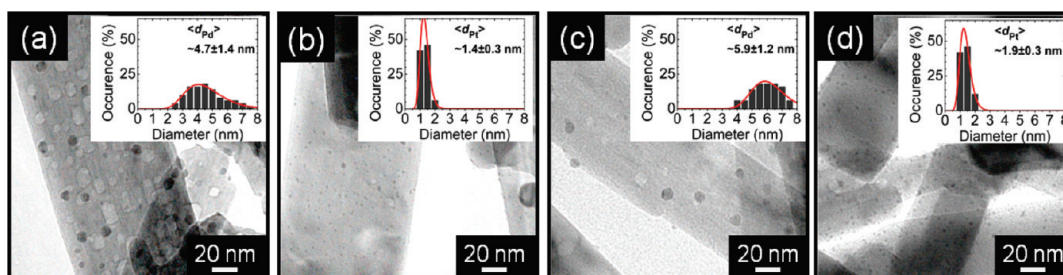
Figure 2. TEM images of (a) N-TiO₂(A)-Pd NF, (b) N-TiO₂(A)-Pt NF, (c) N-TiO₂(B)-Pd NF, and (d) N-TiO₂(B)-Pt NF. In each case, metal loading is ~1.0 wt %. Insets show histograms of the corresponding metal nanoparticle size distributions.

important to point out that a significant amount of sodium ions (Na atom concentration: 8.54 at %) was found in the samples probably due to limited ion exchange in the interior of the initial sodium titanate ($Na_2Ti_yO_{2y+1}$) nanofibers. The presence of Na^+ ions on the surface may influence water molecule adsorption and lead to pH change at the catalyst/aqueous solution interface, thus changing electrochemical potentials in water splitting reactions, and can also be an additional source of charge carriers enhancing or inhibiting photochemical excitation effect. The XPS results on the N content of the samples are consistent with the HR-TEM analysis because the considerable amount of interstitial N atoms may indeed contribute to the expansion of the lattice.

The average ζ-potentials of original TiO₂ NF, N-TiO₂-(A) NF, and N-TiO₂(B) NF measured on powders dispersed in ethanol are −10.14, −18.02, and −16.32 mV, respectively. The somewhat lower potential values (calculated with the Henry equation from the electrophoretic mobility) for the N-doped samples compared to the original TiO₂ NFs suggests slight accumulation of additional negative charge on the surface as a consequence of nitrogen doping.[30]

The as-prepared N-doped TiO₂ nanofibers were finally decorated with Pt and Pd nanoparticles (1 wt % each sample) by wet impregnation with Pt- and Pd-acetylacetonate in acetone followed by drying, thermal decomposition in air at 300 °C for 2 h, and reduction in H₂ flow at 500 °C for 4 h (for details, see Supporting Information). The anatase crystalline

structure is left intact during the metal nanoparticle deposition step as verified by X-ray diffraction (Figure S2). Furthermore, the weak and broadened reflections of Pd(111) and Pt(111) at $2\theta \sim 40.0°$ and Pt(200) at $2\theta \sim 46.5°$ indicate the presence of small nanosized metal particles in the samples (Figure S3).

Analysis of the metal-decorated nanofibers with transmission electron microscopy (TEM) shows that the deposited metal nanoparticles are well-dispersed on the surface (Figure 2). The average size of Pt nanoparticles is considerably smaller than that measured for Pd on both types of supporting surfaces (1.4 ± 0.3 nm on N-TiO₂(A) and 1.9 ± 0.3 nm on N-TiO₂(B) for Pt; and 4.7 ± 1.4 nm on N-TiO₂(A) and 5.9 ± 1.2 nm on N-TiO₂(B) NF for Pd). The particle size is determined by several factors as decomposition of the noble metal source compounds, seed formation rates, and diffusion properties. While both platinum acetylacetonate and palladium acetylacetonate decompose around 200 °C,[31,32] the activation energy of the diffusion of platinum is 1.4−1.5 times higher than that in the case of palladium[33] which leads to a slower surface diffusion of platinum and results in nanoparticle formation from a smaller area around the seed.

Hydrogen production from aqueous ethanol solution with metal-nanoparticle-decorated N-TiO₂(A) NF and N-TiO₂(B) NF catalysts shows about an order of magnitude higher rate than that of the reference catalyst (same support materials without metal) under both UV-A and UV-B irradiation (Figure 3). Using UV-A irradiation, the rates of H₂ evolution were found to be
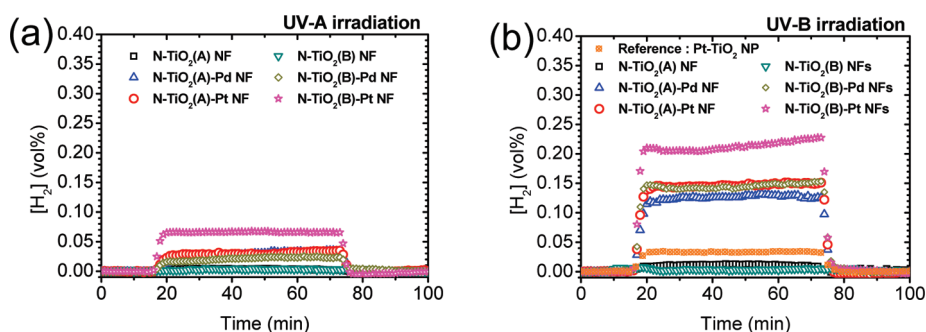
Figure 3. Hydrogen evolution from ethanol/water mixture (molar ratio 1:3) over parent and noble metal loaded (1.0 wt %) catalyst materials (100 mg each) under (a) UV-A (total UV power on the reactor $\sim$1.54 W, $\lambda(I_{max}) \sim$ 365 nm) and (b) UV-B (total UV power on the reactor $\sim$1.46 W, $\lambda(I_{max}) \sim$ 312 nm) irradiation. N_2 gas was bubbled through the reactor at a flow rate of 400 mL/min, serving also as a purging gas for the evolving gaseous products.

around 330 μmol/h for N-TiO$_2$(A)-Pd NF, 330 μmol/h for N-TiO$_2$(A)-Pt NF, 250 μmol/h for N-TiO$_2$(B)-Pd NF, and 700 μmol/h for N-TiO$_2$(B)-Pt NF, while only 50 μmol/h for N-TiO$_2$(A) NF and 30 μmol/h for N-TiO$_2$(B) NF. When using UV-B light source—as expected—the generation rates were considerably higher: 1350 μmol/h for N-TiO$_2$(A)-Pd NF, 1550 μmol/h for N-TiO$_2$(A)-Pt NF, 1530 μmol/h for N-TiO$_2$(B)-Pd NF, and 2250 μmol/h for N-TiO$_2$(B)-Pt NF, and 120 μmol/h for N-TiO$_2$(A) NF and 30 μmol/h for N-TiO$_2$(B) NF. As the catalyst amount was 100 mg in all of the experiment, the hydrogen production rate normalized to the total catalyst mass is 3300 μmol/gh for N-TiO$_2$(A)-Pd NF, 3300 μmol/gh for N-TiO$_2$(A)-Pt NF, 2500 μmol/gh for N-TiO$_2$(B)-Pd NF, and 7000 μmol/gh for N-TiO$_2$(B)-Pt NF, while only 500 μmol/gh for N-TiO$_2$(A) NF and 300 μmol/gh for N-TiO$_2$(B) NF. When using UV-B light source—as expected—the generation rates were considerably higher: 13 500 μmol/gh for N-TiO$_2$(A)-Pd NF, 15 500 μmol/gh for N-TiO$_2$(A)-Pt NF, 15 300 μmol/gh for N-TiO$_2$(B)-Pd NF, and 22 500 μmol/gh for N-TiO$_2$(B)-Pt NF, and 1200 μmol/gh for N-TiO$_2$(A) NF and 300 μmol/h for N-TiO$_2$(B) nanofibers. The highest values of efficiency of the energy conversion from photo energy to chemical energy stored in hydrogen are 5.3 and 10.6% for UV-A and UV-B photons, respectively, calculated by[34]

photo energy conversion (%)

$$= \frac{\text{output energy of hydrogen evolved}}{\text{energy of incident light}} \times 100$$

To further demonstrate the high efficiency of our N-doped and metal-decorated catalysts, commercial TiO$_2$ nanoparticles (Degussa P25) decorated with 1.0 wt % Pt nanoparticles were prepared and their photocatalytic performance was measured using the same conditions as with the nanofiber-based samples. Comparison of the absorption spectra (Figure S4 in Supporting Information) of the TiO$_2$-based materials shows evidence of higher absorptivity in the visible region. As shown in Figure 3b, all of the four new catalysts clearly outperform the conventional TiO$_2$-Pt as well as other

metal-decorated TiO$_2$-based samples synthesized by other groups (Table S1).

The better catalyst activity under UV-B exposure is explained by the larger number of photons of high enough energy to induce electron—hole pairs in the semiconductor. The reason for better photocatalytic activity for the metal-decorated nanofibers as compared to the clean support materials is due to the efficient electron—hole separation, which inhibits recombination, thus improving the photoefficiency of the catalyst.[21−25] Doping TiO$_2$ with nitrogen results in the formation of new p-states near the valence band (similar to deep donor levels in semiconductors), enabling electron transitions with lower energies than in the undoped TiO$_2$.[13] Since the N/Ti ratio for the interstitial N atom of N-TiO$_2$(A) NF is higher than that for the N—Ti bond of N-TiO$_2$(B) NF, one may expect a smaller band gap (or more p-states near the valence band) and consequently a better photocatalytic activity for the catalysts with N-TiO$_2$(A) NF. Experiments with the pristine N-doped support materials are in agreement with the expectations; that is, N-TiO$_2$(A) NF performs better than N-TiO$_2$(B) NF. The metal-decorated samples seem to perform quite similarly except N-TiO$_2$(B)-Pt NF, which produces almost twice as much hydrogen as the other metal-decorated catalysts. This difference is not thoroughly understood; however, a direct electron transition from the p-states to any empty states of the Pt nanoparticle might give a reasonable explanation as such transitions should be more favored energetically than the ones from the valence band and/or the p-states to the conduction band of the semiconductor followed by a subsequent transition to the metal. On the other hand, Pt-decorated samples have advantages over the Pd-decorated ones derived from the smaller particle size and accordingly higher dispersion value of the catalyst particles. To have insight into this aspect, we calculated the turnover frequency values (see the Supporting Information file) and found higher ones for Pt in three of the four cases. As the particle size and dispersion was not fully correlated to the product amount and use of turnover frequency has

controversies in photocatalytic processes, we used product rate/amount of catalyst values for comparing different methods, and this value has the practical advantage to lead easily to product amount/cost of catalyst calculations.

In summary, a set of novel photocatalyst materials based on N-doped TiO_2 nanofibers were developed and tested for hydrogen generation from ethanol–water mixtures of 1:3 molar ratio by applying UV-A and UV-B irradiation. Each photocatalyst was found to be highly efficient, outperforming the metal-decorated conventional TiO_2 nanoparticle catalyst materials.[25,35−40] Among the synthesized photocatalysts, the highest hydrogen generation rates were obtained with N-doped TiO_2(B) nanofibers decorated with Pt nanoparticles (diameter of 1.9 ± 0.3 nm, 1.0 wt % Pt in the catalyst). When we applied only 100 mg of catalyst in 1 L water–ethanol mixture—without optimizing the reactor conditions—the H_2 evolution rates were as high as 700 μmol/h (UV-A) and 2250 μmol/h (UV-B) corresponding to photoefficiency values of ∼3.6 and ∼12.3%, respectively.

METHODS

Sodium titanate ($Na_2Ti_yO_{2y+1}$) nanofibers were synthesized through the hydrothermal synthesis route from anatase TiO_2 in aqueous NaOH solution (10 M) at 175 °C for 24 h using a rotating autoclave applying 120 rpm revolving around its short axis. Washing of $Na_2Ti_yO_{2y+1}$ in 0.1 M HCl was applied to exchange Na^+ ions to protons in the nanofibers. Finally, the product was washed with deionized water to reach pH ∼7 and finally filtered and dried in air at 70 °C.

Two kinds of nitrogen-doped TiO_2 nanofibers, referred as N-TiO_2(A) NF and N-TiO_2(B) NF, were synthesized using different calcination methods. N-TiO_2(A) NF was synthesized by the calcination of $H_{2−x}Na_xTi_yO_{2y+1}$ nanofibers at 600 °C in ammonia gas flow (50 mL/min, 2% NH_3 in N_2 buffer) for 15 h. N-TiO_2(B) NF was synthesized also from $H_{2−x}Na_xTi_yO_{2y+1}$ nanofibers but in two subsequent calcination steps: first, calcined in air at 600 °C for 12 h to form TiO_2 anatase nanofibers, followed by a second calcination step in ammonia gas (50 mL/min, 2% NH_3 in N_2 buffer) at the same temperature for 3 h. The Na/Ti atomic ratios of the two products were ∼30.4% in N-TiO_2(A) NF and ∼25.5% in N-TiO_2(B) NF.

The as-made N-TiO_2(A) NF and N-TiO_2(B) NF were used as support for Pt and Pd nanoparticles deposited by wet impregnation. In a typical process, 20.4 mg of platinum(II) acetylacetonate (Aldrich, 99.99%) or 29.2 mg of palladium(II) acetylacetonate (Aldrich, 99%) was dissolved in 100 mL of acetone and mixed with 1.0 g of N-TiO_2 NF by ultrasonic agitation for 3 h and stirring for 6 h. After the solvents were evaporated at ∼80 °C under N_2 flow, the samples were calcined in air at 300 °C for 2 h, and then reduced in 15% H_2 (in Ar buffer) flow at 500 °C for 4 h to obtain the products: N-TiO_2(A)-Pt, N-TiO_2(A)-Pd, N-TiO_2(B)-Pt, and N-TiO_2(B)-Pd each with ∼1.0 wt % metal load. Pt-decorated TiO_2 nanoparticles (Degussa P25), used as reference catalyst, were made using the same routine as with the nanofibers described above.

The microstructure of diameter/structure of individual nanofibers (N-TiO_2(A) NF and N-TiO_2(B) NF) and the decorating metal nanoparticles (N-TiO_2(A)-Pd NF, N-TiO_2(A)-Pt NF, N-TiO_2(B)-Pd NF, and N-TiO_2(B)-Pt NF) were studied by transmission electron microscopy (EFTEM, LEO 912 OMEGA, 120 kV) as well as by X-ray diffraction (XRD, Siemens D5000 and Philips PW 1380, both using Cu Kα radiation). High-resolution TEM images of TiO_2 NF, N-TiO_2(A) NF, and N-TiO_2(B) NF were taken with a JEOL 2000FX (JEOL Ltd.) electron microscope operated at 200 kV (LaB$_6$ gun).

The ζ-potential of the catalysts (dispersed in ethanol) was determined from their electrophoretic mobility using a ζ-potential analyzer, 90Plus/BI-MAS (Brookhaven Instruments Corporation). The velocity of the particles was measured by laser Doppler velocimetry. The analysis of chemical composition and oxidation state was carried out by X-ray photoelectron spectroscopy (XPS, Kratos Axis Ultra DLD, mono Al Kα source, analysis area of 0.3 × 0.7 mm^2, applying charge neutralizer).

Photocatalytic H_2 generation tests were carried out using 1:3 molar ratio mixture of ethanol and water (1 L) in which 100 mg of TiO_2-based catalyst was suspended before each experiments.

The temperature of the mixture was kept near the room temperature. For light source, six pieces of UV-A lamps (Philips Actinic BL 15W/10 SLV, the wavelength of maximum emission of UV-A lamp was at ∼365 nm and the power in the UV range was ∼3.15 W) or six pieces of UV-B lamps (Sankyo Denki G15T8E UV-B lamps, the wavelength of maximum emission of UV-B lamp was ∼312 nm, and the power in UV range was 3.0 W) were placed in a hexagonal arrangement around the reactor. When the geometry of the experimental setup was taken into account, the total UV-A and UV-B powers reaching the reactor were ∼1.54 and ∼1.46 W, respectively. To avoid sedimentation of the catalyst powders, N_2 gas was bubbled through the reactor with a flow rate of 400 mL/min, serving also as a purging gas for the evolving gaseous products. The outlet of the reactor was connected to a cold trap and to a molecular sieve and then to a hydrogen analyzer (General Electric, XMTC-6C-11).

Supporting Information Available: Photos of original TiO_2 NFs and two different N-doped TiO_2 NF powders; X-ray diffraction patterns of the catalyst samples; normalized absorption spectra of the TiO_2-based materials; table to summarize hydrogen production rates over metal-decorated TiO_2-based photocatalyst materials with corresponding references. This material is available free of charge *via* the Internet at http://pubs.acs.org.

REFERENCES AND NOTES

1. Fujishima, A.; Honda, K. Electrochemical Photolysis of Water at a Semiconductor Electrode. *Nature* **1972**, *238*, 37–38.
2. Fujihira, M.; Satoh, Y.; Osa, T. Heterogeneous Photocatalytic Oxidation of Aromatic-Compounds on TiO_2. *Nature* **1981**, *293*, 206–208.
3. Tseng, H. H.; Wei, M. C.; Hsiung, S. F.; Chiou, C. W. Degradation of Xylene Vapor over Ni-Doped TiO_2 Photocatalysts Prepared by Polyol-Mediated Synthesis. *Chem. Eng. J.* **2009**, *150*, 160–167.
4. Bahnemann, D.; Bockelmann, D.; Goslich, R. Mechanistic Studies of Water Detoxification in Illuminated TiO_2 Suspensions. *Sol. Energy Mater.* **1991**, *24*, 564–583.
5. Konstantinou, I. K.; Albanis, T. A. TiO_2-Assisted Photocatalytic Degradation of Azo Dyes in Aqueous Solution: Kinetic and Mechanistic Investigations—A Review. *Appl. Catal. B* **2004**, *49*, 1–14.
6. Nozik, A. J. Photoelectrolysis of Water Using Semiconducting TiO_2 Crystals. *Nature* **1975**, *257*, 383–386.

7. Zhang, J.; Du, P. W.; Schneider, J.; Jarosz, P.; Eisenberg, R. Photogeneration of Hydrogen from Water Using an Integrated System Based on TiO_2 and Platinum(II) Diimine Dithiolate Sensitizers. *J. Am. Chem. Soc.* **2007**, *129*, 7726–7727.

8. Hoffmann, M. R.; Martin, S. T.; Choi, W. Y.; Bahnemann, D. W. Environmental Applications of Semiconductor Photocatalysis. *Chem. Rev.* **1995**, *95*, 69–96.

9. Li, Q.; Li, Y. W.; Wu, P. G.; Xie, R. C.; Shang, J. K. Palladium Oxide Nanoparticles on Nitrogen-Doped Titanium Oxide: Accelerated Photocatalytic Disinfection and Post-Illumination Catalytic "Memory". *Adv. Mater.* **2008**, *20*, 3717–3723.

10. Gunawan, C.; Teoh, W. Y.; Marquis, C. P.; Lifia, J.; Amal, R. Reversible Antimicrobial Photoswitching in Nanosilver. *Small* **2009**, *5*, 341–344.

11. Yu, H. G.; Irie, H.; Hashimoto, K. Conduction Band Energy Level Control of Titanium Dioxide: Toward an Efficient Visible-Light-Sensitive Photocatalyst. *J. Am. Chem. Soc.* **2010**, *132*, 6898–6899.

12. Kudo, A.; Miseki, Y. Heterogeneous Photocatalyst Materials for Water Splitting. *Chem. Soc. Rev.* **2009**, *38*, 253–278.

13. Asahi, R.; Morikawa, T.; Ohwaki, T.; Aoki, K.; Taga, Y. Visible-Light Photocatalysis in Nitrogen-Doped Titanium Oxides. *Science* **2001**, *293*, 269–271.

14. Sakthivel, S.; Kisch, H. Daylight Photocatalysis by Carbon-Modified Titanium Dioxide. *Angew. Chem., Int. Ed.* **2003**, *42*, 4908–4911.

15. Ohtani, B.; Iwai, K.; Nishimoto, S.; Sato, S. Role of Platinum Deposits on Titanium(IV) Oxide Particles: Structural and Kinetic Analyses of Photocatalytic Reaction in Aqueous Alcohol and Amino Acid Solutions. *J. Phys. Chem. B* **1997**, *101*, 3349–3359.

16. Buso, D.; Pacifico, J.; Martucci, A.; Mulvaney, P. Gold-Nanoparticle-Doped TiO_2 Semiconductor Thin Films: Optical Characterization. *Adv. Funct. Mater.* **2007**, *17*, 347–354.

17. Woan, K.; Pyrgiotakis, G.; Sigmund, W. Photocatalytic Carbon-Nanotube-TiO_2 Composites. *Adv. Mater.* **2009**, *21*, 2233–2239.

18. Hensel, J.; Wang, G. M.; Li, Y.; Zhang, J. Z. Synergistic Effect of Cdse Quantum Dot Sensitization and Nitrogen Doping of TiO_2 Nanostructures for Photoelectrochemical Solar Hydrogen Generation. *Nano Lett.* **2010**, *10*, 478–483.

19. Ratanatawanate, C.; Tao, Y.; Balkus, K. J. Photocatalytic Activity of PbS Quantum Dot/TiO_2 Nanotube Composites. *J. Phys. Chem. C* **2009**, *113*, 10755–10760.

20. Rajeshwar, K.; de Tacconi, N. R.; Chenthamarakshan, C. R. Semiconductor-Based Composite Materials: Preparation, Properties, and Performance. *Chem. Mater.* **2001**, *13*, 2765–2782.

21. Uosaki, K.; Yoneda, R.; Kita, H. Effect of Platinization on the Electrochemical-Behavior of the TiO_2 Electrode in Aqueous-Solutions. *J. Phys. Chem.* **1985**, *89*, 4042–4046.

22. Chen, X.; Mao, S. S. Titanium Dioxide Nanomaterials: Synthesis, Properties, Modifications, and Applications. *Chem. Rev.* **2007**, *107*, 2891–2959.

23. Yoon, J. W.; Sasaki, T.; Koshizaki, N. Dispersion of Nanosized Noble Metals in TiO_2 Matrix and Their Photoelectrode Properties. *Thin Solid Films* **2005**, *483*, 276–282.

24. Park, J. Y.; Renzas, J. R.; Contreras, A. M.; Somorjai, G. A. The Genesis and Importance of Oxide−Metal Interface Controlled Heterogeneous Catalysis; The Catalytic Nanodiode. *Top. Catal.* **2007**, *46*, 217–222.

25. Wu, M.-C.; Sápi, A.; Avila, A.; Szabó, M.; Hiltunen, J.; Huuhtanen, M.; Tóth, G.; Kukovecz, Á.; Kónya, Z.; Keiski, R.; *et al.* Enhanced Photocatalytic Activity of TiO_2 Nanofibers and Their Flexible Composite Films: Decomposition of Organic Dyes and Efficient H_2 Generation from Ethanol−Water Mixtures. *Nano Res.* **2011**, *4*, 360–369.

26. Horvath, E.; Kukovecz, A.; Konya, Z.; Kiricsi, I. Hydrothermal Conversion of Self-Assembled Titanate Nanotubes into Nanowires in a Revolving Autoclave. *Chem. Mater.* **2007**, *19*, 927–931.

27. Wu, M.-C.; Tóth, G.; Sápi, A.; Leino, A.-R.; Kónya, Z.; Kukovecz, A.; Su, W.-F.; Kordás, K. Synthesis and Photocatalytic Performance of Titanium Dioxide Nanofibers and the Fabrication of Flexible Composite Films from Nanofibers. *J. Nanosci. Nanotechnol.* **2011** in press.

28. Okumura, T.; Kinoshita, Y.; Uchiyama, H.; Imai, H. Photoluminescence of Nitrogen-Doped Anatase. *Mater. Chem. Phys.* **2008**, *111*, 486–490.

29. Wang, J.; Tafen, D. N.; Lewis, J. P.; Hong, Z. L.; Manivannan, A.; Zhi, M. J.; Li, M.; Wu, N. Q. Origin of Photocatalytic Activity of Nitrogen-Doped TiO_2 Nanobelts. *J. Am. Chem. Soc.* **2009**, *131*, 12290–12297.

30. Miyauchi, M.; Ikezawa, A.; Tobimatsu, H.; Irie, H.; Hashimoto, K. Zeta Potential and Photocatalytic Activity of Nitrogen Doped TiO_2 Thin Films. *Phys. Chem. Chem. Phys.* **2004**, *6*, 865–870.

31. Kinoshit, K.; Routsis, K.; Bett, J. A. S.; Brooks, C. S. Changes in Morphology of Platinum Agglomerates During Sintering. *Electrochim. Acta* **1973**, *18*, 953–961.

32. Jankovic, B.; Mentus, S. A Kinetic Study of the Nonisothermal Decomposition of Palladium Acetylacetonate Investigated by Thermogravimetric and X-ray Diffraction Analysis Determination of Distributed Reactivity Model. *Metall. Mater. Trans. A* **2009**, *40A*, 609–624.

33. Galeev, T. K.; Bulgakov, N. N.; Savelieva, G. A.; Popova, N. M. Surface-Properties of Platinum and Palladium. *React. Kinet. Catal. Lett.* **1980**, *14*, 61–65.

34. Chen, X. B.; Shen, S. H.; Guo, L. J.; Mao, S. S. Semiconductor-Based Photocatalytic Hydrogen Generation. *Chem. Rev.* **2010**, *110*, 6503–6570.

35. Yang, Y. Z.; Chang, C. H.; Idriss, H. Photo-Catalytic Production of Hydrogen Form Ethanol over M/TiO_2 Catalysts (M = Pd, Pt or Rh). *Appl. Catal. B* **2006**, *67*, 217–222.

36. Sreethawong, T.; Puangpetch, T.; Chavadej, S.; Yoshikawa, S. Quantifying Influence of Operational Parameters on Photocatalytic H-2 Evolution over Pt-Loaded Nanocrystalline Mesoporous TiO_2 Prepared by Single-Step Sol−Gel Process with Surfactant Template. *J. Power Sources* **2007**, *165*, 861–869.

37. Zou, J. J.; He, H.; Cui, L.; Du, H. Y. Highly Efficient Pt/TiO_2 Photocatalyst for Hydrogen Generation Prepared by a Cold Plasma Method. *Int. J. Hydrogen Energy* **2007**, *32*, 1762–1770.

38. Sun, W.; Zhang, S. Q.; Liu, Z. X.; Wang, C.; Mao, Z. Q. Studies on the Enhanced Photocatalytic Hydrogen Evolution over Pt/PEG-Modified TiO_2 Photocatalysts. *Int. J. Hydrogen Energy* **2008**, *33*, 1112–1117.

39. Rosseler, O.; Shankar, M. V.; Du, M. K. L.; Schmidlin, L.; Keller, N.; Keller, V. Solar Light Photocatalytic Hydrogen Production from Water over Pt and Au/TiO_2(Anatase/Rutile) Photocatalysts: Influence of Noble Metal and Porogen Promotion. *J. Catal.* **2010**, *269*, 179–190.

40. Zhang, Z. Y.; Zuo, F.; Feng, P. Y. Hard Template Synthesis of Crystalline Mesoporous Anatase TiO_2 for Photocatalytic Hydrogen Evolution. *J. Mater. Chem.* **2010**, *20*, 2206–2212.